Research Article Vol. 9, No. 6 / June 2022 / Optica 639

OPTICA

Attosecond investigation of extreme-ultraviolet multi-photon multi-electron ionization

M. Kretschmar,[1,†] A. Hadjipittas,[2,†] B. Major,[3,4] J. Tümmler,[1] I. Will,[1] T. Nagy,[1] M. J. J. Vrakking,[1] A. Emmanouilidou,[2,5] and B. Schütte[1,6]

[1]Max-Born-Institut, Max-Born-Strasse 2A, 12489 Berlin, Germany
[2]Department of Physics and Astronomy, University College London, Gower Street, London WC1E 6BT, UK
[3]ELI-ALPS, ELI-HU Non-Profit Ltd., Wolfgang Sandner utca 3., Szeged 6728, Hungary
[4]Department of Optics and Quantum Electronics, University of Szeged, Dóm tér 9, Szeged 6720, Hungary
[5]e-mail: a.emmanouilidou@ucl.ac.uk
[6]e-mail: Bernd.Schuette@mbi-berlin.de

Received 18 February 2022; revised 11 May 2022; accepted 12 May 2022; published 9 June 2022

Multi-electron dynamics in atoms and molecules very often occur on sub- to few-femtosecond time scales. The available intensities of extreme-ultraviolet (XUV) attosecond pulses have previously allowed the time-resolved investigation of two-photon, two-electron interactions. Here we study double and triple ionization of argon atoms involving the absorption of up to five XUV photons using a pair of intense attosecond pulse trains (APTs). By varying the time delay between the two APTs with attosecond precision and the spatial overlap with nanometer precision, we obtain information on complex nonlinear multi-photon ionization pathways. Our experimental and numerical results show that Ar^{2+} is predominantly formed by a sequential two-photon process, whereas the delay dependence of the Ar^{3+} ion yield exhibits clear signatures of the involvement of a simultaneous two-photon absorption process. Our experiment suggests that it is possible to investigate multi-electron dynamics using attosecond pulses for both pumping and probing the dynamics.

https://doi.org/10.1364/OPTICA.456596

1. INTRODUCTION

Strong laser fields can be used to induce multi-electron dynamics in atoms and molecules [1,2]. For example, in the commonly used near-infrared (NIR) regime, techniques such as high-harmonic generation (HHG) spectroscopy have helped to identify multi-electron processes, such as the rearrangement of electrons in molecules upon photoionization [3] and collective multi-electron effects in atoms [4]. However, the use of NIR fields comes at the cost of strongly perturbing the system and involves a strong bending of the atomic and molecular potentials. The high complexity of the contributing processes then often makes a detailed understanding of the underlying physics difficult. A better control over multi-electron dynamics can be achieved by ionizing atoms and molecules using extreme-ultraviolet (XUV) photons, for which ponderomotive effects are small. Even the absorption of a single XUV photon can trigger multi-electron dynamics, e.g., via Auger cascades [5]. Accordingly, XUV-pump XUV-probe experiments are a promising route to provide in-depth understanding of multi-electron dynamics, where one or more photons may be absorbed from both the pump and the probe pulses to produce multiply charged ions. Using state-of-the-art table-top laser technology, such experiments can now be performed with attosecond to few-femtosecond time resolution. Indeed, two-photon, two-electron interactions have been observed with a temporal resolution down to 1.5 fs [6] and 500 as [7].

The absorption of two XUV photons by an atom resulting in its double ionization may occur in either a direct or sequential process. In the latter case, one electron is emitted following the absorption of a first XUV photon, and an intermediate ionic state is formed. Another electron is emitted when a second XUV photon is subsequently absorbed. Various experimental techniques have been applied to distinguish between direct and sequential XUV- or x-ray-induced processes in single-pulse experiments, including intensity-dependent studies and the investigation of recoil-ion momentum distributions [8,9]. Previous experiments further aimed at characterizing XUV pulse duration using a pair of XUV pulses and relied on selecting suitable photon energies that favor direct two-photon-induced two-electron emission over the sequential absorption of two XUV photons [10,11].

In contrast to the relatively simple case of a two-photon absorption process, nonlinear ionization pathways can become very complex when multiple XUV or x-ray photons are absorbed by an atom or a molecule [12–15]. These pathways typically include sequences of one- and multi-photon ionization steps. So far there has been limited direct experimental insight into these multi-photon ionization sequences. Time-resolved investigations of XUV-induced multi-photon ionization with attosecond resolution have been hindered by the lack of suitable light sources. While extremely high XUV intensities can be obtained at free-electron lasers [12], it has only recently become possible to generate

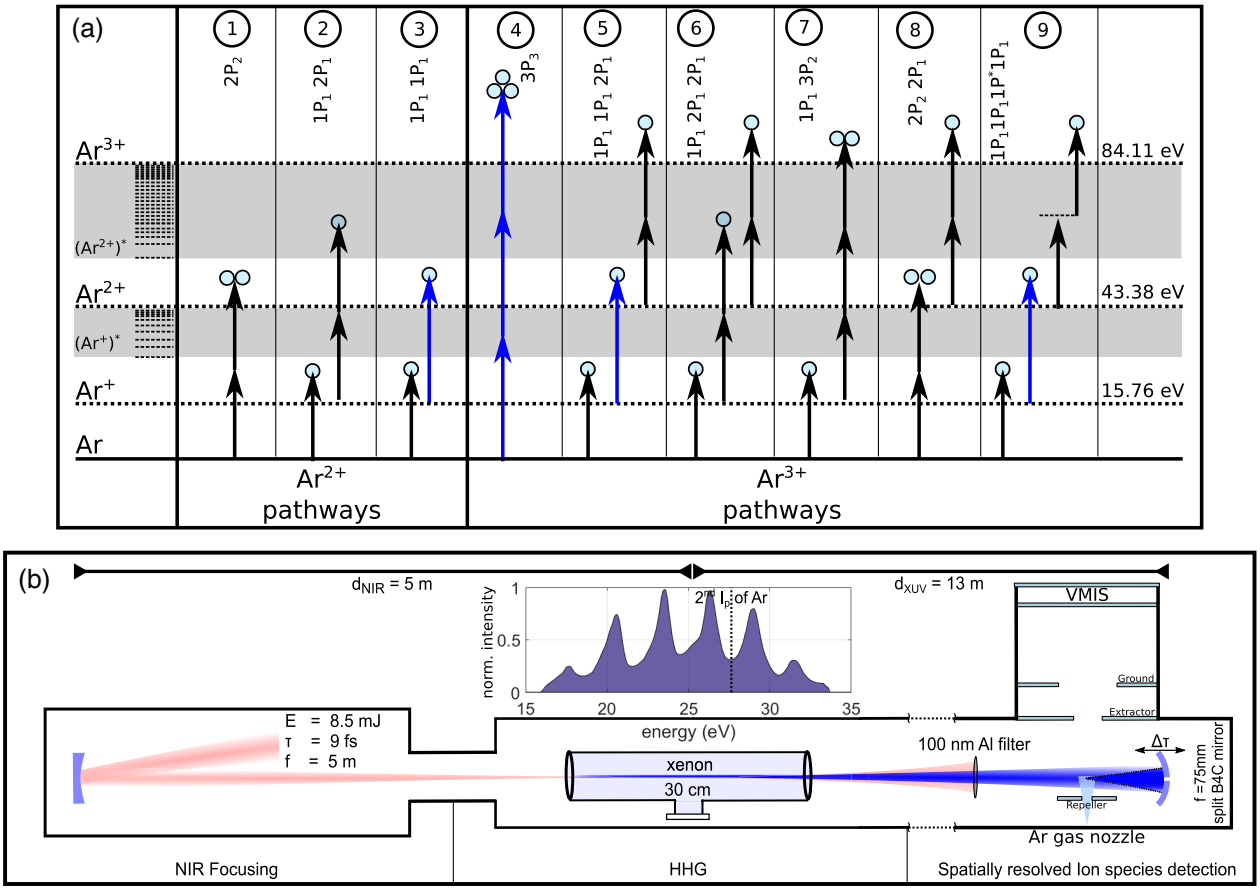

Fig. 1. Multi-photon ionization scheme for Ar and experimental setup. (a) Term scheme showing likely multi-photon ionization pathways leading to the generation of Ar^{2+} and Ar^{3+}, including various direct and sequential ionization pathways (see main text for details). The dashed lines and the gray area indicate a high density of excited states. The notation $N\mathrm{P}_M$ is used to describe an N-photon absorption process leading to the emission of M electrons. The black arrows correspond to XUV photons with an average photon energy of about 25 eV, whereas the blue arrows correspond to XUV photons that have a higher-than-average photon energy, which is required in some of the shown processes. (b) Experimental setup: NIR pulses are focused using a spherical mirror with a focal length of 5 m into a 30-cm-long gas cell filled with Xe. A split spherical B_4C-coated mirror is used to generate two replicas of the APTs and to focus them into the interaction region of a velocity-map imaging spectrometer (VMIS). The XUV photon spectrum obtained from a measured photoelectron spectrum is shown on top.

attosecond pulses and attosecond pulse trains (APTs) at these facilities [16–20]. At the same time, attosecond pulses can be routinely generated using HHG [21]. Recently, intense XUV pulses from HHG sources have been demonstrated, allowing the observation of multi-photon absorption. In Ar and Xe atoms, this has led to the observation of ion charge states up to Ar^{5+} [22–24] and Xe^{5+} [25].

Here we present the results of an XUV-pump XUV-probe experiment in Ar using a pair of APTs with an intensity envelope of ≈3 fs [26], and covering a photon energy range from 16 to 34 eV. Using photons in this photon energy range, Ar^{2+} can be produced by both two- and three-photon processes; see Fig. 1(a). The absorption of two photons may take place in a direct (1) or sequential (3) two-photon process. In the first case, two electrons are emitted following the simultaneous absorption of two photons. In the second case, Ar^+ is formed after the absorption of a first XUV photon, followed by the absorption of a second XUV photon and the emission of a second electron. Ar^{2+} may further be produced by three-photon absorption (2), involving a sequence of a one-photon step leading to Ar^+ and a two-photon process leading to Ar^{2+}. For the generation of Ar^{3+}, six likely pathways are shown, including a direct three-photon process (4) and a fully sequential pathway involving four single-photon absorption steps via intermediate states Ar^+, Ar^{2+}, and Ar^{2+*} (9). Note that a high density of excited states of Ar^{2+} (indicated by the dashed lines and the gray area) lie within the photon energy range of the used APTs [27]. Pathways (5)–(8) involve sequences of one-, two-, and three-photon absorption. Further pathways are possible, but were not found to be important in this work.

To study the nonlinear multi-photon ionization of argon with attosecond resolution, we applied a recently developed XUV intensity scaling scheme using an 18-m-long HHG beamline; see Fig. 1(b) [23]. High harmonics were generated in a 30-cm-long gas cell filled with Xe using 9-fs-long NIR pulses centered around 800 nm from an optical parametric chirped-pulse amplification (OPCPA) system [28]. The carrier–envelope phase (CEP) was not actively stabilized in these measurements, since we expected the influence of the CEP to be small. As shown in Fig. 1(b), two replicas of the APT were generated by a split-and-delay unit. The pulses were focused onto a jet of Ar atoms using a split B_4C-coated spherical mirror with a focal length of 75 mm. An XUV peak intensity of 1×10^{14} W/cm^2 was estimated for each APT (see Section I of Supplement 1). The generated ions were recorded using a velocity-map imaging spectrometer (VMIS) [29] that was operated in spatial-map imaging mode [30].

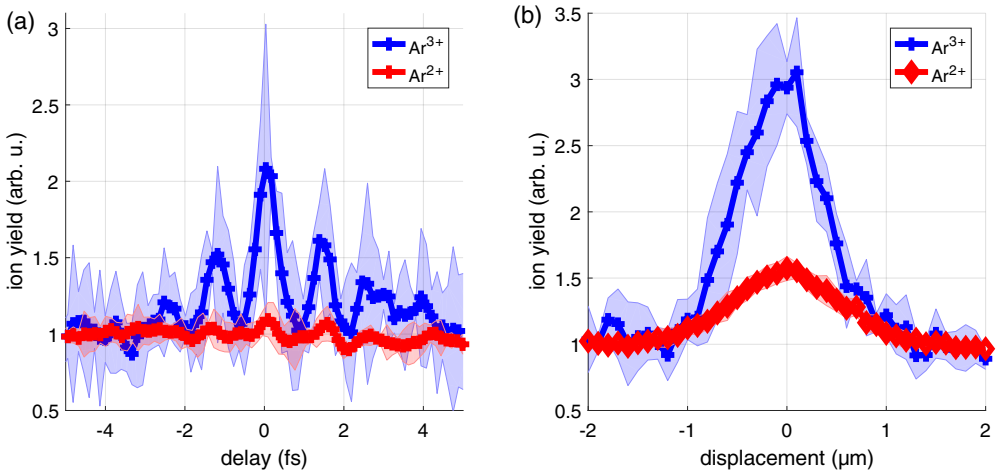

Fig. 2. Measured Ar^{2+} and Ar^{3+} ion yields as a function of the XUV-XUV temporal and spatial overlap. (a) The Ar^{2+} ion yield (red curve) is only weakly modulated as a function of the XUV-XUV time delay, whereas clear oscillations with a period of 1.3 fs are observed in the delay-dependent Ar^{3+} ion yield (blue curve). Standard deviations obtained from four scans are shown by the red- and blue-shaded areas. The signal from 1600 laser shots was integrated at each delay point, and the measured number of Ar^{2+} and Ar^{3+} ions per delay point was of the order of 10^5 and 10^3, respectively. (b) At a delay of 20 fs between the two APTs, the Ar^{2+} ion yield (red curve) is enhanced by a factor of 1.6 when the XUV pulses spatially overlap, while an enhancement of three is observed for Ar^{3+} (blue curve). Standard deviations obtained from four scans are shown by the red- and blue-shaded areas. The combination of these results shows that the formation of Ar^{2+} is dominated by a sequential pathway, whereas both sequential and direct processes are important for the generation of Ar^{3+}.

In what follows, we will present measurements of the Ar^{2+} and Ar^{3+} yields as a function of both the delay and spatial overlap between the two APTs. Our aim is to identify the dominant mechanisms responsible for the Ar^{2+} and Ar^{3+} formation [see Fig. 1(a)] on the basis of the measured dependencies. To do so, we will compare the measured dependencies with results of theoretical calculations including the mechanisms shown in Fig. 1(a). It should be emphasized that theoretical modeling of the experiment is extremely challenging, since the experiment collects signals from an extended focal volume where the two APTs overlap and interfere with each other, leading to a complicated XUV intensity and pulse shape distribution within the focal volume. Furthermore, it is crucial to take into account the broad bandwidth of the APTs, which in this work was done using a Monte Carlo method. This requires much higher computational efforts than solving rate equations which are often applied in studies of this kind [31]. Since, as a result, the computation of focal volume averaged results within this model is unfeasible, we have first characterized the role of focal volume averaging in a simplified model, where we have calculated non-resonant two-photon ionization using XUV pulses obtained in a previous simulation using realistic NIR pulses [26]. These calculations show that to a good approximation, the experiment can be considered and modeled as an intensity autocorrelation (see Section II of Supplement 1). Therefore, this approximation will be used within this paper.

2. RESULTS

We performed two types of measurements. In the first type, the two APTs were spatially overlapped, and the time delay between them was varied. The measured Ar^{2+} and Ar^{3+} ion yields as a function of the XUV-XUV time delay are presented in Fig. 2(a). The Ar^{2+} yield (red curve) exhibits only weak oscillations with a relative oscillation amplitude of about 10%, whereas the Ar^{3+} ion yield (blue curve) shows strong oscillations where at optimal overlap the yield is twice the yield of non-overlapping pulses. The period of oscillations is about 1.3 fs, which corresponds to half the oscillation period of the NIR laser and suggests a strong enhancement of the Ar^{3+} yield when individual attosecond pulses in the pump and probe APTs overlap. In the second type of measurement, the two APTs were delayed by 20 fs with respect to each other, and the focus position of one of the APTs was scanned laterally. As shown in Fig. 2(b), the Ar^{2+} ion yield was increased by a factor of 1.6, and the Ar^{3+} ion yield was increased by a factor of three when the APTs spatially overlapped. Taken together, these experiments allow us to better understand the importance of both direct and sequential multi-photon processes.

To assess the relative importance of direct and sequential processes, we first of all make the observation (which is based on the aforementioned focal volume averaged simulations; see Section II of Supplement 1) that, except at zero delay, sequential two-photon two-electron ionization does not depend on the delay. In contrast, direct two-photon, two-electron ionization is about twice as efficient when the APTs temporally overlap as opposed to when they do not. We stress that this result is obtained only when realistic APTs resulting from simulations of our XUV source are used, while a Fourier limited APT would still provide small temporal modulations for a sequential two-photon two-electron ionization process. It thus follows from the Ar^{2+} ion yields [red curve in Fig. 2(a)] obtained at zero overlap and when the APTs do not temporally overlap that at least 10% of the Ar^{2+} yield is due to direct ionization, whereas up to 90% is due to sequential processes. With regard to the second experiment, where the two APTs were delayed by 20 fs with respect to each other, we argue that in the absence of ground-state depletion, the yield of Ar^{2+} resulting from direct ionization does not depend on whether or not the two APTs are spatially overlapped. By contrast, given that sequential ionization scales quadratically with the fluence, it is expected that the contribution from sequential ionization doubles when the two APTs spatially overlap (see Section III of Supplement 1). It follows that the 60% increase in the Ar^{2+} yield in the latter case

suggests that at least 60% of the Ar^{2+} formation occurs by means of a sequential process and up to 40% by a direct process. Combining both observations, we thus estimate that about 10%–40% of the Ar^{2+} formation occurs by direct two-photon two-electron emission, and the remainder by sequential processes. The weak delay dependence further indicates that pathway (2) does not play an important role. We note that sequential and direct processes may also occur via resonant states [32,33]. However, when assuming that the lifetimes of the resonantly excited states are long compared to the APT duration, we do not expect excited states to change the analysis of our results in terms of sequential and direct two-photon absorption.

The experimental results for Ar^{3+} suggest that its formation takes place in a sequence of two to three steps, of which at least one step involves the absorption of two or more XUV photons. Due to the large number and the complexity of the possible pathways, a definite assignment to one of the pathways shown in Fig. 1(a) is not possible. However, when one makes the assumption that Ar^{3+} is generated via the Ar^{2+} ground state (i.e., the first two XUV photons are preferentially absorbed sequentially by two one-photon processes), this excludes all pathways except (5) and (9). The strong modulation of the Ar^{3+} ion yield as a function of the time delay [Fig. 2(a)] further excludes pathway (9), suggesting that pathway (5) dominates. The analysis that Ar^{2+} is formed by a two-photon process and Ar^{3+} is formed by a four-photon process is consistent with our intensity-dependent studies reported in Ref. [23]. We note that the result of the intensity autocorrelation shown in Fig. 2(a) cannot be used to reconstruct the pulse structure without making additional assumptions. We make, however, the observation that a simulation of an autocorrelation trace based on our simulated attosecond pulse structure [see Fig. 4(a)] exhibits features similar to the delay-dependent Ar^{3+} ion yield measurement shown in Fig. 2(a). The duration of the individual attosecond bursts within the simulation lies between 400 and 500 as.

Deeper insights into the nonlinear multi-photon ionization of Ar can be obtained by modeling, which will be described in the following. To be able to account for the broad bandwidth of the XUV pulses, a Monte Carlo technique was developed that computed the final ion yields and the pathways leading to the formation of the ions. Single-photon and direct two- and three-photon ionization processes were accounted for (see Section IV of Supplement 1 for details). In the simulations, a pair of short APTs was used [see gray-shaded area in Fig. 4(a)], as previously obtained from HHG simulations [26]. To keep the calculations feasible (considering the broad bandwidth of the APTs and the fact that the simulations had to be performed for a set of delays), resonant excitations [32,33] were not taken into account. We do not expect this, however, to alter the main conclusions.

The simulated Ar^{2+} and Ar^{3+} ion yields as a function of the time delay between the two APTs are presented in Fig. 3(a). While the Ar^{2+} ion yield exhibits weak oscillations with an amplitude of about 10%, the Ar^{3+} ion yield strongly oscillates and is about twice as high at zero delay as compared to the case of non-overlapping pump and probe pulses. Considering the high degree of complexity of both the experiments and simulations, these results are in good agreement with the experimental observations [Fig. 2(a)].

The contributions of different pathways leading to the generation of Ar^{2+} and Ar^{3+} are shown in Figs. 3(b) and 3(c). The formation of Ar^{2+} [Fig. 3(b)] is dominated by a sequential pathway involving two single-photon absorption steps [blue curve, pathway (3) in Fig. 1(a)], and shows almost no delay dependence. Further contributions stem from pathways (1) (red curve) and (2) (black curve), which involve a direct two-photon absorption step. These contributions are responsible for the weak oscillations observed in Fig. 3(a). The dominance of a two-photon sequential pathway as obtained from the simulations is consistent with the analysis of the experimental results.

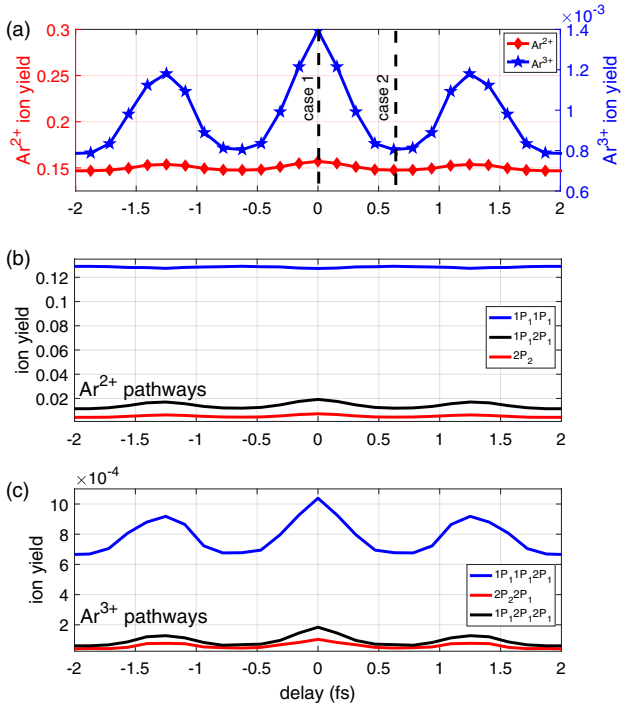

Fig. 3. Simulated Ar^{2+} and Ar^{3+} ion yields as a function of the XUV-XUV time delay. (a) The simulated Ar^{2+} ion yield (red curve) exhibits small delay-dependent changes of about 10%, while the relative Ar^{3+} ion yield (blue curve) varies by a factor of almost two. These results are in good agreement with the experimental results shown in Fig. 2. Case 1 and case 2 are two time delays for which the time-dependent ion formation is shown in Fig. 4(b). Contributions to the Ar^{2+} ion yield as a function of XUV-XUV time delay, dominated by sequential two-photon absorption (blue curve), which hardly shows any delay dependence. (c) The Ar^{3+} ion yield (blue curve) is dominated by a sequence of two one-photon and one two-photon absorption steps [pathway (5) in Fig. 1(a)]. All pathways contributing to the formation of Ar^{3+} show clear oscillatory behavior as a function of the XUV-XUV time delay.

The generation of Ar^{3+} [Fig. 3(c)] is found to be dominated by a three-step sequence of two one-photon and one two-photon absorption processes via intermediate states Ar^{+} and Ar^{2+} [blue curve, pathway (5) in Fig. 1(a)]. Pathways (6) (black curve) and (8) (red curve) also contribute to the overall Ar^{3+} ion yield. All these contributions exhibit clear oscillations as a function of the XUV-XUV time delay. We note that in our simplified model, we found that a sequence of three ionization steps results in an increased ion yield by a factor of four, when the two APTs are spatially, but not temporally overlapped (see Section III of Supplement 1). Therefore, the experimental observations, which showed an increase in Ar^{3+} ion yield by a factor of three at spatial overlap and an additional increase of a factor of two at temporal overlap between the two APTs, are consistent with pathway (5) playing an important role for the formation of Ar^{3+}, as predicted by the Monte Carlo simulations.

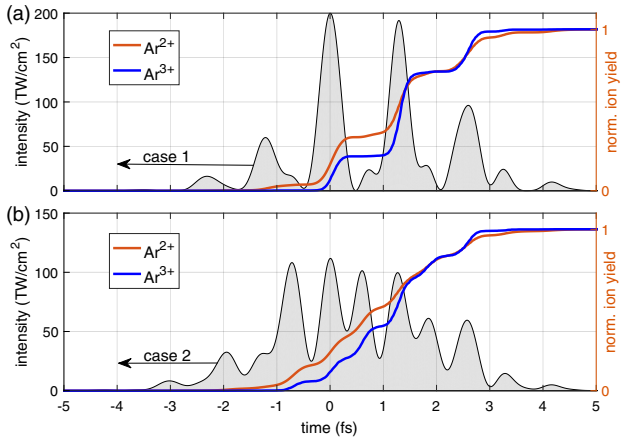

Fig. 4. Simulated evolution of the Ar^{2+} and Ar^{3+} ion yields in time. The results are normalized with respect to the final ion yields and are shown for XUV-XUV delays of (a) 0 fs (case 1 in Fig. 3) and (b) 0.66 fs (case 2 in Fig. 3); see the gray-shaded areas for the corresponding effective XUV pulses. In both cases, ionization occurs in a stepwise fashion due to the APT structure.

The numerical simulations provide information on the formation of Ar^{2+} and Ar^{3+} ions in the time domain. The corresponding results are presented in Fig. 4 for XUV-XUV time delays of (a) 0 fs and (b) 0.66 fs (see the gray-shaded areas for the corresponding effective XUV pulse structures). As a result of the APT structure, the ion formation occurs in steps in both cases. The increase in Ar^{3+} ion yield in Fig. 4(a) is particularly large in the temporal window between 1.1 and 1.6 fs. This is a consequence of the fact that the Ar^{3+} ion formation depends on both the instantaneous Ar^{2+} ion population and the instantaneous XUV intensity.

3. DISCUSSION AND OUTLOOK

Our results demonstrate that the application of intense APTs enables a better understanding of complex multi-photon ionization pathways. In our study, the combination of temporally and spatially resolved measurements applied to different ionic species made it possible to separately study the role of direct and sequential multi-photon processes.

The high XUV intensities obtained in our experiment furthermore pave the way for attosecond-pump attosecond-probe spectroscopy at higher XUV photon energies, a regime that is typically difficult to access because of low HHG conversion efficiencies. This could make it possible to study multi-electron dynamics and electron–electron correlation following the removal of core electrons in atoms and molecules with attosecond resolution. Examples include the study of Auger cascades and double Auger decay processes, in which the relaxation of a valence-shell electron to an inner-shell vacancy leads to the sequential or simultaneous emission of two Auger electrons [5]. By performing spatially dependent measurements of the ion yields at different time delays, a complete picture of complex ionization pathways can be obtained, including simultaneous and sequential multi-photon absorption and the role played by the decay of inner-shell vacancies.

Funding. European Commission (GINOP-2.3.6-15-2015-0000); KIFÜ; Leverhulme Trust Research Project (2017-376); Legion Computational Resources.

Acknowledgment. We thank Valer Tosa for providing his HHG simulation code. A. E. thanks Peter Lambropoulos for useful discussions. A. E. further acknowledges the use of the Legion computational resources at UCL. We acknowledge KIFÜ for awarding us access to resources based in Hungary in Debrecen and Szeged. The ELI-ALPS project (GINOP-2.3.6-15-2015-00001) is supported by the European Union and co-financed by the European Regional Development Fund.

Disclosures. The authors declare no conflicts of interest.

Data availability. Data underlying the results presented in this paper are not publicly available at this time but may be obtained from the authors upon reasonable request.

Supplemental document. See Supplement 1 for supporting content.

[†]These authors contributed equally to this paper.

REFERENCES

1. G. Mainfray and G. Manus, "Multiphoton ionization of atoms," Rep. Prog. Phys. **54**, 1333–1372 (1991).
2. T. Brabec and F. Krausz, "Intense few-cycle laser fields: frontiers of nonlinear optics," Rev. Mod. Phys. **72**, 545–591 (2000).
3. O. Smirnova, Y. Mairesse, S. Patchkovskii, N. Dudovich, D. Villeneuve, P. Corkum, and M. Y. Ivanov, "High harmonic interferometry of multi-electron dynamics in molecules," Nature **460**, 972–977 (2009).
4. A. Shiner, B. Schmidt, C. Trallero-Herrero, H. J. Wörner, S. Patchkovskii, P. B. Corkum, J. Kieffer, F. Légaré, and D. Villeneuve, "Probing collective multi-electron dynamics in xenon with high-harmonic spectroscopy," Nat. Phys. **7**, 464–467 (2011).
5. F. Penent, J. Palaudoux, P. Lablanquie, L. Andric, R. Feifel, and J. H. D. Eland, "Multielectron spectroscopy: the xenon 4*d* hole double auger decay," Phys. Rev. Lett. **95**, 083002 (2005).
6. P. Tzallas, E. Skantzakis, L. Nikolopoulos, G. D. Tsakiris, and D. Charalambidis, "Extreme-ultraviolet pump–probe studies of one-femtosecond-scale electron dynamics," Nat. Phys. **7**, 781–784 (2011).
7. E. J. Takahashi, P. Lan, O. D. Mücke, Y. Nabekawa, and K. Midorikawa, "Attosecond nonlinear optics using gigawatt-scale isolated attosecond pulses," Nat. Commun. **4**, 2691 (2013).
8. R. Moshammer, Y. H. Jiang, L. Foucar, A. Rudenko, T. Ergler, C. D. Schröter, S. Lüdemann, K. Zrost, D. Fischer, J. Titze, T. Jahnke, M. Schöffler, T. Weber, R. Dörner, T. J. M. Zouros, A. Dorn, T. Ferger, K. U. Kühnel, S. Düsterer, R. Treusch, P. Radcliffe, E. Plönjes, and J. Ullrich, "Few-photon multiple ionization of Ne and Ar by strong free-electron-laser pulses," Phys. Rev. Lett. **98**, 203001 (2007).
9. A. Rudenko, L. Foucar, M. Kurka, T. Ergler, K. U. Kühnel, Y. H. Jiang, A. Voitkiv, B. Najjari, A. Kheifets, S. Lüdemann, T. Havermeier, M. Smolarski, S. Schössler, K. Cole, M. Schöffler, R. Dörner, S. Düsterer, W. Li, B. Keitel, R. Treusch, M. Gensch, C. D. Schröter, R. Moshammer, and J. Ullrich, "Recoil-ion momentum distributions for two-photon double ionization of He and Ne by 44 eV free-electron laser radiation," Phys. Rev. Lett. **101**, 073003 (2008).
10. Y. Nabekawa, H. Hasegawa, E. J. Takahashi, and K. Midorikawa, "Production of doubly charged helium ions by two-photon absorption of an intense sub-10-fs soft x-ray pulse at 42 eV photon energy," Phys. Rev. Lett. **94**, 043001 (2005).
11. R. Mitzner, A. A. Sorokin, B. Siemer, S. Roling, M. Rutkowski, H. Zacharias, M. Neeb, T. Noll, F. Siewert, W. Eberhardt, M. Richter, P. Juranic, K. Tiedtke, and J. Feldhaus, "Direct autocorrelation of soft-x-ray free-electron-laser pulses by time-resolved two-photon double ionization of He," Phys. Rev. A **80**, 025402 (2009).
12. A. A. Sorokin, S. V. Bobashev, T. Feigl, K. Tiedtke, H. Wabnitz, and M. Richter, "Photoelectric effect at ultrahigh intensities," Phys. Rev. Lett. **99**, 213002 (2007).
13. L. Young, E. P. Kanter, B. Krässig, *et al.*, "Femtosecond electronic response of atoms to ultra-intense x-rays," Nature **466**, 56–61 (2010).
14. B. Rudek, S.-K. Son, L. Foucar, *et al.*, "Ultra-efficient ionization of heavy atoms by intense x-ray free-electron laser pulses," Nat. Photonics **6**, 858–865 (2012).
15. A. Rudenko, L. Inhester, K. Hanasaki, *et al.*, "Femtosecond response of polyatomic molecules to ultra-intense hard x-rays," Nature **546**, 129–132 (2017).

16. N. Hartmann, G. Hartmann, R. Heider, *et al.*, "Attosecond time–energy structure of x-ray free-electron laser pulses," Nat. Photonics **12**, 215–220 (2018).
17. P. K. Maroju, C. Grazioli, M. Di Fraia, *et al.*, "Attosecond pulse shaping using a seeded free-electron laser," Nature **578**, 386–391 (2020).
18. J. Duris, S. Li, T. Driver, *et al.*, "Tunable isolated attosecond x-ray pulses with gigawatt peak power from a free-electron laser," Nat. Photonics **14**, 30–36 (2020).
19. J. T. O'Neal, E. G. Champenois, S. Oberli, *et al.*, "Electronic population transfer via impulsive stimulated x-ray Raman scattering with attosecond soft-x-ray pulses," Phys. Rev. Lett. **125**, 073203 (2020).
20. S. Li, T. Driver, P. Rosenberger, *et al.*, "Attosecond coherent electron motion in Auger-Meitner decay," Science **375**, 285–290 (2022).
21. F. Krausz and M. Ivanov, "Attosecond physics," Rev. Mod. Phys. **81**, 163–234 (2009).
22. A. Nayak, I. Orfanos, I. Makos, M. Dumergue, S. Kühn, E. Skantzakis, B. Bodi, K. Varju, C. Kalpouzos, H. I. B. Banks, A. Emmanouilidou, D. Charalambidis, and P. Tzallas, "Multiple ionization of argon via multi-XUV-photon absorption induced by 20-GW high-order harmonic laser pulses," Phys. Rev. A **98**, 023426 (2018).
23. B. Senfftleben, M. Kretschmar, A. Hoffmann, M. Sauppe, J. Tümmler, I. Will, T. Nagy, M. J. J. Vrakking, D. Rupp, and B. Schütte, "Highly nonlinear ionization of atoms induced by intense high-harmonic pulses," J. Phys. Photon. **2**, 034001 (2020).
24. B. Major, O. Ghafur, K. Kovács, K. Varjú, V. Tosa, M. J. J. Vrakking, and B. Schütte, "Compact intense extreme-ultraviolet source," Optica **8**, 960–965 (2021).
25. B. Bergues, D. E. Rivas, M. Weidman, A. A. Muschet, W. Helml, A. Guggenmos, V. Pervak, U. Kleineberg, G. Marcus, R. Kienberger, D. Charalambidis, P. Tzallas, H. Schröder, F. Krausz, and L. Veisz, "Tabletop nonlinear optics in the 100-eV spectral region," Optica **5**, 237–242 (2018).
26. B. Major, M. Kretschmar, O. Ghafur, A. Hoffmann, K. Kovács, K. Varjú, B. Senfftleben, J. Tümmler, I. Will, T. Nagy, D. Rupp, M. J. J. Vrakking, V. Tosa, and B. Schütte, "Propagation-assisted generation of intense few-femtosecond high-harmonic pulses," J. Phys. Photon. **2**, 034002 (2020).
27. A. Kramida, Y. Ralchenko, and J. Reader, and NIST ASD Team, "NIST atomic spectra database (ver. 5.1)," National Institute of Standards and Technology, 2013, Online. Available: http://physics.nist.gov/asd, September 8, 2014.
28. M. Kretschmar, J. Tuemmler, B. Schütte, A. Hoffmann, B. Senfftleben, M. Mero, M. Sauppe, D. Rupp, M. J. J. Vrakking, I. Will, and T. Nagy, "Thin-disk laser-pumped OPCPA system delivering 4.4 TW few-cycle pulses," Opt. Express **28**, 34574–34585 (2020).
29. A. T. J. B. Eppink and D. H. Parker, "Velocity map imaging of ions and electrons using electrostatic lenses: Application in photoelectron and photofragment ion imaging of molecular oxygen," Rev. Sci. Instrum. **68**, 3477 (1997).
30. M. Stei, J. von Vangerow, R. Otto, A. H. Kelkar, E. Carrascosa, T. Best, and R. Wester, "High resolution spatial map imaging of a gaseous target," J. Chem. Phys. **138**, 214201 (2013).
31. G. M. Nikolopoulos and P. Lambropoulos, "Multiple ionization of neon under soft x-rays: theory versus experiment," J. Phys. B **47**, 115001 (2014).
32. E. V. Gryzlova, R. Ma, H. Fukuzawa, *et al.*, "Doubly resonant three-photon double ionization of Ar atoms induced by an EUV free-electron laser," Phys. Rev. A **84**, 063405 (2011).
33. M. D. Kiselev, P. A. Carpeggiani, E. V. Gryzlova, S. M. Burkov, M. Reduzzi, A. Dubrouil, D. Faccialá, M. Negro, K. Ueda, F. Frassetto, F. Stienkemeier, Y. Ovcharenko, M. Meyer, M. D. Fraia, O. Plekan, K. C. Prince, C. Callegari, G. Sansone, and A. N. Grum-Grzhimailo, "Photoelectron spectra and angular distribution in sequential two-photon double ionization in the region of autoionizing resonances of ArII and KrII," J. Phys. B **53**, 244006 (2020).